INTERFACE

royalsocietypublishing.org/journal/rsif

Research

Cite this article: Caetano DLZ, de Carvalho SJ, Metzler R, Cherstvy AG. 2020 Critical adsorption of multiple polyelectrolytes onto a nanosphere: splitting the adsorption–desorption transition boundary. *J. R. Soc. Interface* **17**: 20200199.
http://dx.doi.org/10.1098/rsif.2020.0199

Received: 24 March 2020
Accepted: 3 June 2020

Subject Category:
Life Sciences–Physics interface

Subject Areas:
nanotechnology, biotechnology, biophysics

Keywords:
nanoparticles, polyelectrolytes, electrostatics, critical adsorption, phase-transition boundary

Author for correspondence:
Andrey G. Cherstvy
e-mail: a.cherstvy@gmail.com

Electronic supplementary material is available online at https://doi.org/10.6084/m9.figshare.c.5021537.

THE ROYAL SOCIETY PUBLISHING

Critical adsorption of multiple polyelectrolytes onto a nanosphere: splitting the adsorption–desorption transition boundary

Daniel L. Z. Caetano[1,2,3], Sidney J. de Carvalho[1], Ralf Metzler[4] and Andrey G. Cherstvy[4]

[1]São Paulo State University (UNESP), Institute of Biosciences, Humanities and Exact Sciences, Campus São José do Rio Preto, 15054-000 Brazil
[2]Institute of Chemistry, and [3]Center for Computational Engineering and Sciences, State University of Campinas (UNICAMP), 13083-970 Campinas, Brazil
[4]Institute for Physics and Astronomy, University of Potsdam, 14476 Potsdam-Golm, Germany

DLZC, 0000-0002-0476-3115; SJdC, 0000-0002-9763-2797; RM, 0000-0002-6013-7020; AGC, 0000-0002-0516-9900

Employing extensive Monte Carlo computer simulations, we investigate in detail the properties of multichain adsorption of charged flexible polyelectrolytes (PEs) onto oppositely charged spherical nanoparticles (SNPs). We quantify the conditions of critical adsorption—the phase-separation curve between the adsorbed and desorbed states of the PEs—as a function of the SNP surface-charge density and the concentration of added salt. We study the degree of fluctuations of the PE–SNP electrostatic binding energy, which we use to quantify the emergence of the phase subtransitions, including a series of partially adsorbed PE configurations. We demonstrate how the phase-separation adsorption–desorption boundary shifts and splits into multiple subtransitions at low-salt conditions, thereby generalizing and extending the results for critical adsorption of a single PE onto the SNP. The current findings are relevant for finite concentrations of PEs around the attracting SNP, such as the conditions for PE adsorption onto globular proteins carrying opposite electric charges.

1. Introduction

The adsorption of polyelectrolytes (PEs) onto charged interfaces of different geometries [1–6] has numerous applications, e.g. for surface coating, in biotechnology as gene-delivery vectors, for stabilization of colloids, in biophysics and pharmacology, in the food industry, for paper-making and for water-purification purposes. The adsorption of PEs onto micelles, dendrimers, globular proteins and lipid membranes was also studied [7–12]. Moreover, the wetting, lubrication and adhesive properties of certain surfaces can be controlled and tuned via PE coating and formation of responsive PE layers [5].

Starting from the pioneering theoretical studies of *critical* adsorption of a single long flexible PE chain onto an oppositely charged plane with the Debye–Hückel attractive potential by Wiegel [13,14] and Muthukumar & von Goeler [2,15], the adsorption–desorption conditions onto planar and curved interfaces have been extensively investigated in recent decades theoretically [2,3,6,13,15–25], experimentally [7–12,26–31] and by computer simulations [25,32–36] (see the recent review [37]). Various characteristics of PE–surface adsorption—the behaviour above the critical-adsorption point—in different surface geometries, in the presence of various physical PE–interface interactions and for varying polymer flexibilities (e.g. flexible, semiflexible and kink-able chains)—were examined in detail as well [3,6,12,16,37–69].

PEs get adsorbed onto an oppositely charged interface when the benefit from reducing the overall electrostatic (ES) energy via binding or complexation overwhelms the free-energy penalty associated with the more confined

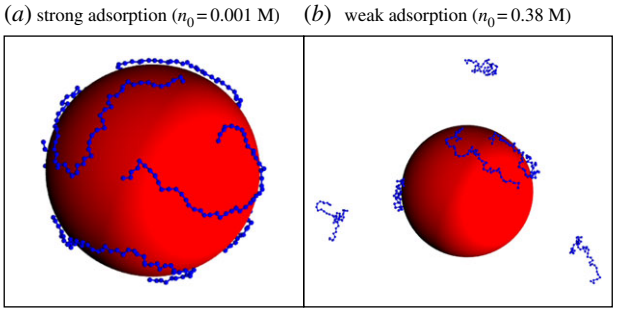

Figure 1. Typical conformations of six PE chains near the attractive SNP shown for the regimes of (*a*) strong and (*b*) weak adsorption. The SNPs are not shown to scale.

(adsorbed) states of the polymer [6,13,17,20] (figure 1). The linear [20] and nonlinear [36] Poisson–Boltzmann theories were used to describe the PE–surface attractive ES potential. The adsorption onto heterogeneous/patchy [4,19,45,70–73], multicomponent responsive [68] and low-dielectric [21,74,75] interfaces was also considered. The conditions of critical adsorption under confinement [21,22,25], for pH-sensitive or titratable PEs [35] (see also [37,62,63,65,76,77]), block copolymers [78] and polyampholyte chains [35,63,79] were examined by theory and simulations as well. Recently, we quantified the conditions of critical PE adsorption onto dipolar Janus-type net-neutral spherical nanoparticles (SNPs) [24].

Some of these situations revealed significant differences from the standard conditions of critical PE adsorption onto planar [2,13] and spherical [6,15,17,20] interfaces. These differences are important, e.g. for rationalizing the experimental evidence of critical adsorption of PEs onto oppositely charged globular proteins [10,12,26,27,59], micelles [7,9,80], dendrimers [8,81], liposomes [31] and colloids [29,30]. The critical single-chain PE–surface adsorption was examined by quantum-mechanical methods in the three basic geometries [6,20] and for low-dielectric adsorbing interfaces [21]. The latter is a standard situation in PE-adsorption experiments onto mica and silica surfaces, for complexation of PEs (including DNA) with certain proteins[1] as well as for adsorption of PE complexes [82] and DNA [83–86] onto lipid membranes.

In our previous studies of PE critical adsorption onto oppositely charged surfaces only *single-chain* systems were considered. This mimics the case of infinite dilution of PEs in experiments and reproduces the respective single-chain theoretical limit [6,17,18,20,21,23–25,36,79]. The classical Debye–Hückel screening in the electrolyte solution was implemented (with anion and cation concentrations equal to n_0 for 1 : 1 salt). In reality, PE concentrations are always finite, making the consideration of *multichain adsorption* more relevant. Additionally, especially for relatively high PE concentrations, the effects of PE-own counterions—contributing to the overall charge neutrality—become gradually more important.

A number of adsorption properties of flexible PEs onto oppositely charged planar and curved interfaces as well as SNPs were considered [53,55,56,61,63,65]. One application of current findings is PE adsorption onto and PE complex formation with the oppositely charged molecules (e.g. aggregation of PEs with globular proteins). Similar to our previous studies [24,25,79], we employ here extensive Monte Carlo computer simulations to uncover the features of critical adsorption for multiple PE chains at varying solution salinity and SNP surface-charge density. As a

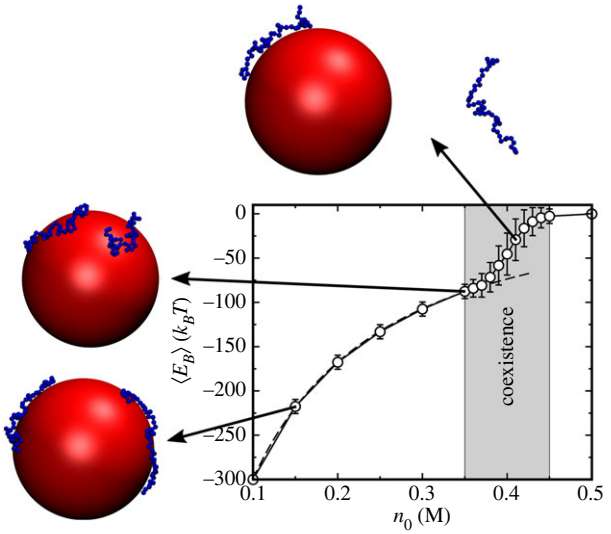

Figure 2. Mean PE–SNP ES binding energy $\langle E_B \rangle$ in units of thermal energy k_BT plotted as a function of salt concentration n_0, with some representative configurations of the PE chains observed in simulations being presented. The grey area in the graph defines the region of coexistence of adsorbed and desorbed PEs. The dashed curve at low salt is the variation of $\langle E_B(n_0) \rangle$ given by equation (3.2) (see text for details). The error bars quantify the ES binding-energy fluctuations, which are amplified in the coexistence region, as detailed in electronic supplementary material, figure S3. Parameters: the surface-charge density of the SNP of radius $a = 100$ Å is $\sigma = -0.1$ C m^{-2}, the number of PE chains is $M = 2$ and the PE polymerization degree is $N = 50$.

reference case, we compare these new phase-transition results with the conditions of critical adsorption of a single PE onto a uniformly charged SNP.

The paper is organized as follows. In §2, we outline the physical model used in the simulations and describe theoretical approximations employed in the analysis. In §3, we present the main results of computer simulations and discuss the underlying trends and their physical rationales. We conclude in §4 with an overview possible future developments.

2. Potentials and methods

The model system is composed of M PE chains in the vicinity of an oppositely charged SNP, as illustrated in figures 1 and 2. The whole system is enclosed by a large spherical cavity (to make the simulations feasible and to minimize the effects of confinement onto polymer conformations). The cavity radius R_{cav} used in the simulations is 10^4 Å, i.e. approximately 10^2 times larger than the PE contour length. The size effects of such a simulation cell are negligible (even larger cavities yield the same results). For this cavity size the polymer volume-density is approximately 10^{-12} Å^{-3} in the case of six adsorbing PEs. The system is immersed into an aqueous solution of 1 : 1 salt with a bulk concentration of ions n_0 and relative dielectric constant $\epsilon_s = 78.7$, kept at the temperature $T = 298.15$ K. Each PE chain is modelled as a fully flexible and non-stretchable polymer of N spherical beads (monomers) of radius $b = 2$ Å. Each bead carries the charge $q_i = +e_0$, where e_0 is the elementary charge. Neighbouring charges are separated in the simulations by a fixed distance equal to the Bjerrum length, $l_B = e_0^2/(4\pi\epsilon_0\epsilon_s k_B T) \approx 7$ Å (in SI units; in the Gaussian system $4\pi\epsilon_0 = 1$), where ϵ_0 is the absolute permittivity and k_B is the Boltzmann constant. The own counterions of the PEs and SNP are included in the total solution salinity to maintain the overall charge neutrality in simulations. Water

molecules are modelled implicitly, while the PE chains are simulated explicitly at each step.

The repulsive ES interactions between the ith and jth monomers of the PE located at radius-vectors $\mathbf{r}_i$ and $\mathbf{r}_j$ are given by the screened Coulomb potential. The monomer–monomer (m-m) Debye–Hückel potential is

$$U_{\mathrm{m-m}}(r_{ij}) = \begin{cases} \infty, & r_{ij} < 2b, \\ \dfrac{1}{4\pi\epsilon_0\epsilon_s}\dfrac{q_i q_j e^{-\kappa r_{ij}}}{r_{ij}}, & \text{otherwise.} \end{cases} \tag{2.1}$$

Here

$$\kappa^{-1} = \lambda_D = \frac{1}{\sqrt{4\pi l_B(2n_0 + |n_{\mathrm{PEs}} - n_{\mathrm{SNP}}|)}} \tag{2.2}$$

is the Debye screening length in the electrolyte solution containing the added 1 : 1 salt with the total concentration of anions and cations $2n_0$, as well as with concentrations of PE- and SNP-own monovalent counterions, $n_{\mathrm{PEs}} = M \times N/(\frac{4}{3}\pi R_{\mathrm{cav}}^3)$ and $n_{\mathrm{SNP}} = 4\pi a^2|\sigma|/(\frac{4}{3}\pi R_{\mathrm{cav}}^3)$, correspondingly; see also [87]. The contribution of the PEs and SNP counterions is computed based on the *net* electric charge of the PE–SNP system. All point-size ions and counterions in the solution are modelled implicitly via their 'mean-field action' through the value of the reciprocal Debye screening length, κ; see equation (2.2).[2]

The SNP has the surface-charge density σ and radius $a = 100$ Å. Attractive ES Debye–Hückel potentials of the SNP with the ith PE monomer at distance $r_i = |\mathbf{r}_i|$ from the sphere centre (the monomer–particle (m-p) potential) are given by [6,15,17,20,21]

$$U_{\mathrm{m-p}}(r_i) = \begin{cases} \infty, & r_i < a + b, \\ \dfrac{1}{4\pi\epsilon_s\epsilon_0}\dfrac{4\pi a^2\sigma q_i}{1+\kappa a}\dfrac{e^{-\kappa(r_i-a)}}{r_i}, & \text{otherwise.} \end{cases} \tag{2.3}$$

Similar to [24,25,33–36,78,79], Metropolis Monte Carlo simulations in the *NVT* ensemble are employed below.

Three different movements of the polymer are implemented in order to sample the conformational space and calculate the averaged adsorption characteristics: (i) translational random displacements of the whole PE chain, (ii) randomly chosen pivot rotations for a given chain, and (iii) randomly chosen crankshaft motions [88].[3] The equilibration process is carried out after running the system for approximately 10^7 simulation steps, while the averaged properties are calculated below using 10^7 statistically independent configurations of the PEs around the SNP.

Specifically, the equilibration process is carried out by running two independent simulations with different initial conditions. In the first one, all PE chains start fully contacting the SNP, while in the second simulation all PEs start at random locations in the surrounding solution. After 10^7 simulation steps, we verify the convergence between the average properties obtained from these two simulation runs, and the process is repeated until the required degree of convergence is reached. For the case of no convergence after 10^7 steps, we start a new run using with the last recorded polymer configuration from the previous run as the initial configuration and repeat this procedure until convergence.

Below, we examine the properties of critical PE–SNP adsorption for *multichain* systems (figures 1 and 2). The video files illustrating the polymer adsorption–desorption dynamics are presented in the electronic supplementary material. The video files numbered as {1, 2, 3} and {4, 5, 6} illustrate the PE–nanosphere adsorption for the case of two and six polymer chains, respectively, with the salt concentration in each set taking the values $n_0 = 1$, 10 and 380 mM, correspondingly. Each of these files contains 10^4 frames recorded for the SNP surface-charge density $\sigma = -0.1$ C m^{-2}. The entire simulation box is shown and, therefore, at high-salt conditions with mostly desorbed PE chains the SNPs appear smaller in the videos. Note that rapid motions of PEs seen in the course of dynamics for the free chains stem from the high acceptance rate of pivot and crankshaft movements (used both for equilibration and for reaching a quicker convergence of the mean statistical properties to be computed).

3. Results

3.1. Two PE chains

First, we remind the reader that the classical PE–plane critical-adsorption result states that [13] the adsorbed state is preferred (in the presence of the exponentially screened ES potential) for charge densities larger than the critical value, $|\sigma| > |\sigma_c|$, scaling with the solution salinity as

$$|\sigma_c(\kappa)| \sim \kappa^3. \tag{3.1}$$

Physically, upon increasing κ the PE–plane ES attraction is diminished and larger surface-charge densities should be maintained to trigger PE–surface adsorption [6,13,17,20]. Various modifications of the law (3.1) are known to exist, e.g. for curved [2,6,15,24] and patterned [70,71] interfaces, Janus particles [24], PE chains of a finite length, PE adsorption onto proteins and dendrimers [9,12,29] and for the nonlinearly (rather than linearly) treated ES PE–surface attractive potentials [36]. Below, we unveil certain modifications and pronounced splitting of the critical-transition boundaries for multichain PE adsorption onto SNP: the results that extend/modify the single-chain adsorption law (3.1). We show that—due to the interplay of PE–SNP attractive and PE–PE repulsive ES interactions—a splitting of the adsorption–desorption transition emerges.

Figure 2 shows some typical conformations of two PE chains for varying solution salinity as well as the variation of the mean ES PE–SNP binding energy, $\langle E_B\rangle$. The latter is computed via summing the $U_{\mathrm{m-p}}$ potentials (2.3) over all the PEs' monomers and averaged over all polymer configurations encountered in the simulations. Naturally, at lower salt concentration the adsorbed PE state is preferable because of stronger ES PE–SNP attractions. Electronic supplementary material, figure S1*a* shows the time series of the PE–SNP ES binding energy of two PEs ($M = 2$) for $\sigma = -0.1$ C m^{-2}. This representation makes obvious the sharp transitions along the time series between the (2-0) state (two PEs are adsorbed), the (1-1) state (one PE is adsorbed and one desorbed) and the (0-2) state (both PEs are desorbed) of the chains. We can identify a range of salinities—the grey area in the inset of figure 2—within which the variation of $\langle E_B\rangle$ with n_0 does not obey the laws of standard exponential screening given by equation (2.3). This is shown in figure 2 at salt concentrations lower than the region of adsorption–desorption coexistence (see also fig. 1*a* of [33]). The dashed curve in figure 2 corresponds to the Debye–Hückel-type function for the mean ES binding energy, namely

$$\langle E_B(n_0)\rangle = \alpha e^{-\beta n_0^{1/2}}, \tag{3.2}$$

with the fit parameters $\alpha \approx -1220\, k_BT$ and $\beta \approx 4.44\ \mathrm{M}^{-1/2}$. Here, the molar concentration M is not to be confused with the number of PEs, M. The discontinuous transitions between the adsorbed PE–SNP state at low salinities and desorbed state at larger salinities is characterized by clear deviations from the expected behaviour (3.2) for the PE–nanosphere ES binding energy.

The probability distribution of E_B for the simulated time series is shown in electronic supplementary material, figure S1*b*. The total probabilities are normalized to unity (as they should) when the contribution of the binding energy from the desorbed state (the vertical 'line' in this figure) is taken into account. For two PEs near the ES-attractive SNP we identify three coexisting states: (i) two PEs are adsorbed, with the total ES binding energy $E_B \approx -80\ k_BT$, (ii) one PE is adsorbed, with $E_B \approx -35\ k_BT$, and (iii) both PEs are desorbed, with a weak binding, $E_B \approx 0\ k_BT$. These values are the averages of instantaneous binding energies over the time periods the PEs spend in the respective states in our computer simulations.

Electronic supplementary material, figure S2 shows the probability of occurrence of these three *c*oexisting *s*tates (denoted by the subscript 'cs' below) for varying salt concentration n_0. Note that the data for electronic supplementary material, figure S1*b* were obtained at $n_0 = 0.39$ M via counting the number of PE configurations in each of the substates (visualized by the time series shown in electronic supplementary material, figure S1*a*). The probability of each substate (with a distinct range of the PE–SNP ES binding energies, as shown in electronic supplementary material, figure S1*b*) in this PE–SNP system, denoted as $p(E_B)$, is proportional to these numbers. This counting procedure has been repeated for systematically varying n_0 to restore the variation of the probability of each of the PE–SNP adsorption substates, denoted as $P_{\mathrm{cs}}^{n=\{2,1,0\}}(n_0)$, upon addition of salt into the system, as shown in electronic supplementary material, figure S2 (the CPU time to produce this figure on a standard workstation is approximately one week).

As more salt is added in the solution, polymer configurations with two PEs being adsorbed get replaced by states with one PE adsorbed and one PE desorbed, and, finally, states with the two PE chains being desorbed start to dominate. The exact values of n_0 at which these (2-0)→(1-1) and (1-1)→(0-2) adsorption–desorption subtransitions take place depend on the PE linear-charge density e_0/l_{B}, the SNP radius a and its surface-charge density σ.[4] Naturally, at a given n_0, the sum of all three probabilities is unity,

$$P_{\mathrm{cs}}^{2} + P_{\mathrm{cs}}^{1} + P_{\mathrm{cs}}^{0} = 1. \tag{3.3}$$

Electronic supplementary material, figure S3 illustrates the fluctuations of the total PE–SNP binding energy at $\sigma = -0.1\,\mathrm{C\ m^{-2}}$. Similar to figure 2, the region of state coexistence around $n_0 \approx 0.4$ M is shown in grey. In this region, as follows from electronic supplementary material, figure S2, the number of transitions between the (2-0), (1-1) and (0-2) states is maximized (their probabilities at this point are ≈1/4, ≈1/2 and ≈1/4, respectively). These frequent transitions give rise to large changes of E_B in the simulations that, in turn, result in a dramatic increase of ES-binding-energy fluctuations,

$$\delta E_B = \sqrt{\langle E_B^2 \rangle - \langle E_B \rangle^2}. \tag{3.4}$$

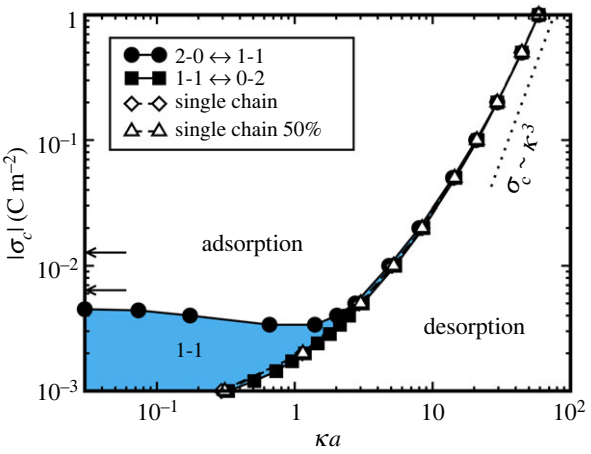

Figure 3. Magnitude of the critical SNP surface-charge density $|\sigma_c|$ for adsorption of two PEs versus the reciprocal Debye screening length, κ. The open diamonds and open triangles are the result of simulations for critical adsorption of a single PE onto the SNP obtained with the criterion of maximal ES-energy fluctuations and with 50%/50% of time for the PE to stay in the adsorbed and desorbed states, respectively (these two datasets yield almost superimposing symbols). The theoretical prediction of equation (3.1) is the dotted line in the high-salt limit. The arrows denote the charge densities at which one and two adsorbed PEs fully neutralize the SNP charge. The blue region shapes the range of $|\sigma_c|$ and κa in between the boundaries of (2-0)→(1-1) and (1-1)→(0-2) adsorption–desorption subtransitions.

At a chosen SNP surface-charge density, σ, the amount of added salt at which the ES-energy fluctuations are maximal is associated with the respective adsorption–desorption critical subtransition. Hereafter, we implement this adsorption–desorption criterion (as compared, for instance, with the standard criterion of 50% adsorbed and 50% desorbed PE configurations along the recorded time series in the simulations). The criterion based on ES-energy fluctuations, as we show below, enables the exact determination and categorization of the adsorption–desorption subtransitions for multichain PE–SNP complexation. This is the main goal and achievement of the current study, making it more general (or superior) to our previous simulations of single-chain PE–surface critical adsorption [24,25,36,79].

It is natural to define the critical n_0 for the subtransitions (2-0)→(1-1) and (1-1)→(0-2) at the points of *maximal* δE_B for the respective partially adsorbed states; see electronic supplementary material, figure S4.[5] This is the key methodology to determine adsorption–desorption subtransitions for the multiple-PEs system we develop and employ here for the first time.[6] Recalculating the respective values $\kappa_{(2\text{-}0)\to(1\text{-}1)}$ and $\kappa_{(1\text{-}1)\to(0\text{-}2)}$ of the reciprocal Debye lengths via equation (2.2) at each σ value, and repeating this procedure for systematically varying σ in the simulations, gives rise to a splitting of the adsorption–desorption boundary $|\sigma_c(\kappa)|$ into $|\sigma_c(\kappa_{(2\text{-}0)\to(1\text{-}1)})|$ and $|\sigma_c(\kappa_{(1\text{-}1)\to(0\text{-}2)})|$ subtransitions. Within the blue region in figure 3, the number of transitions between the three coexisting states of the PE chains is maximized. The blue region is situated 'inside' the corresponding grey region of figure 2 for the same model parameters. Namely, at a given SNP surface-charge density the blue region in figure 3 indicates the range of solution salinities in between the two maxima of the binding-energy fluctuations, $p(\delta E_B)$, realized for the respective subtransitions (see electronic supplementary material, figure S5 for the case

of six PEs). The results for adsorption of a *single* PE onto the same SNP—obtained with the same adsorption criterion of maximal ES-energy fluctuations—are shown as the open diamonds in figure 3.

Note that the grey area in electronic supplementary material, figure S4 denotes the region of state coexistence, while the critical-adsorption subtransitions shaping the blue region of figure 3 take place at the two points inside the respective grey area. Specifically, the transitions are realized at the maxima of the ES binding-energy fluctuations; see the peaks of $p(\delta E_B)$ in electronic supplementary material, figure S4.

The single-PE results based on the adsorption criterion of 50% adsorbed and 50% desorbed PE configurations are also shown in figure 3 (as the open triangles). As one can see, the single-chain critical-adsorption results for $|\sigma_c(\kappa)|$ for these two adsorption criteria are almost superimposing. The adsorption criterion based on ES-energy fluctuations, however, enables us to find the critical-adsorption boundaries of all partially adsorbed PE–SNP states and to determine *subtransitions* for multichain PE–SNP adsorption.

Remarkably, we find that at intermediate salinities the trend of increasing $|\sigma_c|$ with increasing κ observed for two SNP-adsorbing PEs at high salt gets reverted, and at very small κ values the value of $|\sigma_c|$ for the (2-0)→(1-1) subtransition ultimately saturates at a plateau. This splitting of the adsorption–desorption boundary into distinct subtransitions and a plateau-like behaviour of $|\sigma_c(\kappa)|$ at vanishing salt are the novel results. Naturally, for critical-adsorption conditions for six PEs these new features become enriched, as we quantify below.

3.2. Six PE chains

Extending the consideration for two PEs in §3.1, we perform the same analysis for six PEs and seven possible partially adsorbed states, namely (6-0), (5-1), (4-2), (3-3), (2-4), (1-5) and (0-6). In figure 4*a*, we present the computed probabilities of these coexisting states (at a given SNP surface-charge density σ) for varying concentrations of added salt n_0. As expected, at low amounts of added salt all PE chains are adsorbed onto the oppositely charged sphere (strong PE–SNP ES attraction, $n = 6$), while for increasing n_0 values progressively smaller numbers of PE chains are adsorbed, down to $n = 0$ at high-salt conditions. In figure 4, the range of salt concentrations where the subtransitions are realized for $M = 6$ chains is shown for $\sigma = -0.1$ C m^{-2}; at each n_0 the sum of the probabilities of all the partially adsorbed PE states is unity.[7]

The maximal fluctuations of the PE–SNP ES-binding energy, δE_B, are observed in the narrow regions of the respective subtransitions between the neighbouring substates of the partially adsorbed PEs; see figure 4*b* for some and electronic supplementary material, figure S5 for all the subtransitions. The procedure in the multichain system is similar to the two-chain analysis in §3.1: the input data for state coexistence and binding-energy fluctuations should now be treated for each subtransition separately. The complications are due to the complexity of this six-chain system and because some energy-fluctuation curves contain two (or more) local maxima. The characteristics of the system in figure 4 for $\sigma = -0.01$ C m^{-2} and -0.002 C m^{-2} are further detailed in electronic supplementary material, figures S6 and S7, respectively. At all conditions studied in the simulations, we observed a clear correspondence between the points of

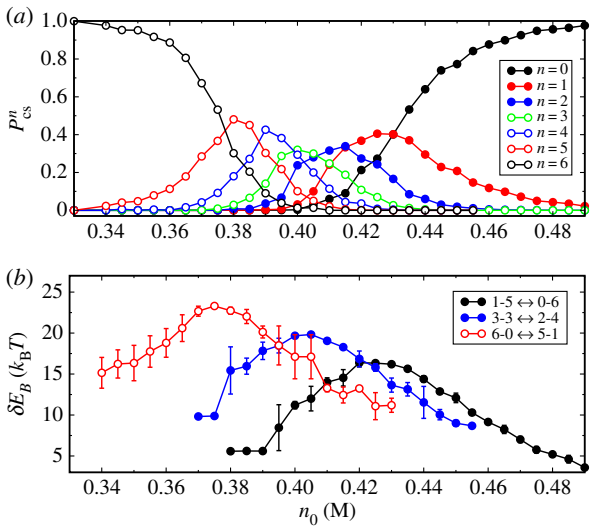

Figure 4. (*a*) Probabilities P^n_{cs} of partially adsorbed PE–SNP states for $M = 6$ chains. (*b*) Respective fluctuations of the PE–SNP ES-binding energy for some of the subtransitions (with the error bars). Parameters: $\sigma = -0.1$ C m^{-2} and $N = 50$.

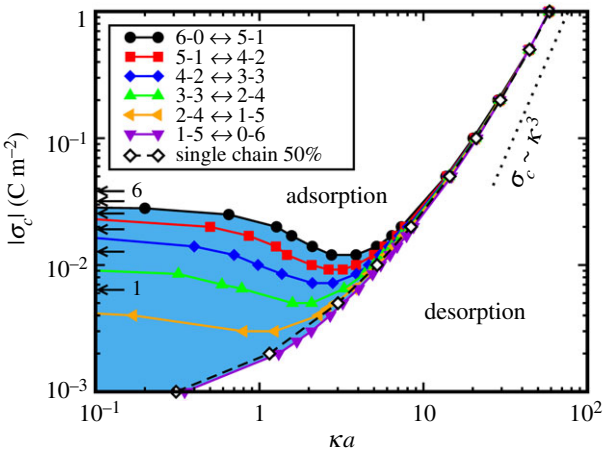

Figure 5. Critical SNP surface-charge density $|\sigma_c|$ for adsorption of $M = 6$ PEs (with $N = 50$ monomers) obtained from the δE_B-based adsorption criterion plotted versus κa. The data for single-PE critical adsorption with the standard 50%/50% adsorbed/desorbed criterion for PEs are also included as open diamonds. The six arrows on the vertical axis indicate the $|\sigma|$ values at which the SNP is completely neutralized by one to six PE chains fully adsorbed onto its surface.

maxima of the ES binding-energy fluctuations and of crossing of the state-probability curves for the respective substates. This makes our new methodology for determining the critical-adsorption subtransitions in the system of multiple SNP-adsorbing PEs physically valid and universal.[8]

The sequential adsorption of PEs we observe in figure 4*a* is reflected in a splitting of the adsorption–desorption boundary: the dependence of the critical surface-charge density of the SNP $|\sigma_c|$ on the concentration of added salt now splits into M subtransitions and different dependencies for the critical SNP surface-charge densities for each of them are observed (figure 5). This splitting of the single-chain $|\sigma_c(\kappa)|$ boundary in the low-salt limit is our main result for critical adsorption of multiple PEs onto the ES-attractive SNP. The critical-adsorption results for a single PE obtained in the simulations employing the 50%/50% adsorbed/desorbed criterion are shown in figure 5 (open diamonds, as in figure 3).

We emphasize that the total simulation time for figures 3 and 5—for critical adsorption of two and six PE chains—

would amount to ≈8 months on a standard modern personal computer: a computer cluster with ≈500 cores was therefore used for these large-scale simulations.

We observe that at high concentrations of added salt the scaling dependence $|\sigma_c(\kappa)|$ for the respective subtransitions is almost insensitive to the number of adsorbed PEs. In this limit, the Debye screening length is much shorter than the SNP radius so that each PE chain adsorbs locally almost without noticing—owing to strong screening of PE–PE repulsion—the ES repulsions stemming from the already adsorbed PEs. The required $|\sigma_c|$ in this situation of local PE adsorption is relatively large and the total charge of all the PE chains is much smaller than the magnitude of the SNP charge, $|Q_{\mathrm{SNP}}| = 4\pi a^2|\sigma|$.

In stark contrast, at low concentrations of added salt n_0 and for relatively small $|\sigma|$ the effect of splitting into the adsorption–desorption subtransitions is very pronounced. This is due, in part, to a partial compensation of the SNP charge by the already adsorbed PEs. In this limit, the Debye screening length can be much longer than the SNP radius, $1/\kappa \gg a$, so that each PE upon adsorption 'feels' the charge of the already SNP-deposited polymers. During this 'obstructed adsorption', the PE chains in the solution experience effectively weaker ES attraction to the SNP (the situation of global adsorption due to SNP charge renormalization by the already adsorbed PEs).[9] Physically, at low salt the adsorption of additional PEs will acquire progressively larger $|\sigma|$, as indeed observed in the phase diagram of the subtransitions $((j)\text{-}(M-j)) \rightarrow ((j \pm 1)\text{-}(M-j \mp 1))$ in figure 5. To construct this phase diagram, extensive computer simulations at systematically varying σ were performed and at each σ-point shown in figure 5 the separation of the polymer configurations into the coexisting (partially adsorbed) states was enumerated, as per the procedure shown in figure 4. This enabled us to quantify all the PE–SNP adsorption subtransitions.

The data from the computer simulations in figure 5 show that for the (6-0)→(5-1) subtransition the value of $|\sigma_c|$ starts deviating from the results for (single PE)–SNP adsorption at $\kappa \lesssim 0.1/\text{Å}$, while for the (2-4)→(1-5) subtransition some splitting of $|\sigma_c(\kappa)|$ is observed at considerably smaller amounts of salt, $\kappa \lesssim 0.03/\text{Å}$. We also observe that after the initial decrease of $|\sigma_c(\kappa)|$ with decreasing κ the adsorption–desorption boundary for each subtransition starts to *rise* again at $\kappa a \approx 1 \ldots 3$ and at very small κ values the respective values $|\sigma_c|$ reach plateaus. The magnitude of these plateaus depends on the (average) number of adsorbed PE chains for a given adsorption subtransition. At vanishing κ values this plateau-like behaviour of $|\sigma_c|$ is physically expected: with no screening present in the system at $\kappa \rightarrow 0$, the ES PE–SNP interactions become nearly insensitive to any further decrease in the solution salinity. Clearly, depending on the actual system parameters, this upward trend of $|\sigma_c(\kappa)|$ as the solution salinity decreases and the plateau-like behaviour of $|\sigma_c(\kappa)|$ at very small κ might also occupy a quite extensive region of the adsorption–desorption diagram. Here, the ratio of the SNP charge to the total charge of all the PEs is the determining factor, $\eta = 4\pi a^2|\sigma|/(M \times e_0 N)$.[10]

In figure 5 in the region of small κ, we indicate by the arrows the $|\sigma|$ values at which the SNP is fully neutralized upon adsorption of a given number of PE chains. In this low-salt regime for all the subtransitions a *substantial overcharging* of the SNP by the adsorbed PEs is detected, possibly because of finite-size effects of the adsorbed PEs. The region of SNP surface-charge densities where the plateau-like behaviour of $|\sigma_c|$ emerges in our simulations is partly superimposed with the region of SNP charge neutralization by a given number of PEs; see the arrows on the vertical axis of figure 5. Owing to PE–SNP overcharging effects, the blue region in figure 5 illustrating the region of $|\sigma_c|$ and κa within which all the adsorption–desorption subtransitions take place is lower in terms of $|\sigma|$ than the region of SNP charge neutralization (which is situated in between arrows 1 and 6 in figure 5). Figure 5 presents the key results of the current study.

The renormalized SNP charge for the adsorption–desorption subtransition $((j)\text{-}(M-j)) \rightarrow ((j-1)\text{-}(M-j+1))$ can be assessed as

$$|Q^{\mathrm{eff}}_{\mathrm{c,SNP}}(\kappa, j)| \approx 4\pi a^2|\sigma_c(\kappa, j)| - f(j-1/2)e_0 N \mathrm{e}^{-\kappa b}. \qquad (3.5)$$

In this expression, with $j = \{6, 5, 4, 3, 2, 1\}$, the reduction of the critical SNP charge is due to $\approx(j-1/2)$ PE chains being tightly adsorbed (on average) for the respective subtransition involving between j and $(j-1)$ adsorbed PEs. This PE charge enters equation (3.5) with the Debye–Hückel screening factor $\mathrm{e}^{-\kappa b}$ (here b is the monomer radius). The fit coefficient f in equation (3.5) physically means the fraction of the PE charge efficiently participating in SNP neutralization. For $f < 1$ only with a fraction of the PEs' charge effectively neutralizes the SNP (for instance, at some times PEs can be relatively far from the sphere).

The 'optimal' value of f is found numerically to ensure the closest superposition of the critical-adsorption curves, $|\sigma_c(\kappa, j)|$, for all the subtransitions in the region of large salinities. Naturally, the optimal-fit f-value depends on the actual model parameters controlling ES interactions, such as the sphere radius a, the polymerization degree N, the inter-monomer distance along the PE, etc. We find that the results for $|Q^{\mathrm{eff}}_{c,}\mathrm{SNP}(\kappa, j)|$ display nearly universal dependence for all the subtransitions at intermediate-to-large κ-values. At low salinities, in contrast, the plateaus of $|\sigma_c|$ remain pronounced and thus no universal curve for $|Q^{\mathrm{eff}}_{c,}\mathrm{SNP}(\kappa, j)|$ emerges, as shown in electronic supplementary material, figure S8. Note that the goodness-of-$\sigma_c(\kappa)$-data fit by ansatz (3.5) is sensitive to the exact value of f, in particular when the SNP charge is comparable to the charge of all the partially adsorbed PEs (the region of small $|\sigma_c|$ and small κ). For large κ and large $|\sigma_c|$, as $\eta \gg 1$ the fit is nearly f-insensitive.

Finally, we study the density distribution of PE monomers away from the SNP, $\rho(r)$, and the width of the adsorbed PE layer, w, for the condition $|\sigma| > |\sigma_s|$, i.e. above the adsorption transition. The width w is defined in standard fashion [6,20], as the width of the peak of the PE-monomer distribution $\rho(r)$ measured at its half-height. Intuitively, larger $|\sigma|$ values yield more SNP-localized PE conformations and thinner PE layers (see electronic supplementary material, figure S9*a*), while the value of w increases near and diverges at the adsorption–desorption 'demarcation' boundary. We find that at high n_0 the adsorbed PEs feel only weakly the presence of the already adsorbed PEs. As our PE chains are rather short, they adsorb onto the SNP surface often without 'overlaps' and the thickness of the adsorbed layer for multiple PEs is only slightly larger than that for a single PE adsorbed at the same σ; see electronic supplementary material, figure S9*b*. The error bars for w are often smaller than the symbol size (not shown).

By contrast, at low salt concentrations—and for the SNP surface-charge densities still above the borderline for

adsorption of all six PE chains—the adsorption of each PE gives rise to a thicker adsorbed layer on the sphere surface. In this situation, the already deposited PEs renormalize the SNP charge, diminishing its adsorption propensity; see equation (3.5). The system is being rendered closer to the adsorption–desorption boundary, with expectedly less compact layers of the adsorbed PEs (e.g. figs. 3 and 5 of reference [20]), as shown in electronic supplementary material, figure S9*b* for the current data for two and six SNP-adsorbing PEs.

4. Discussion and conclusions

We conducted extensive Monte Carlo simulations to unravel the critical-adsorption characteristics for the ES-driven adsorption of multiple PE chains onto an oppositely charged SNP. Our main result is the methodology based on the maximization of the ES-energy fluctuations for determining and exact quantification of the adsorption subtransitions (split phase-transition boundaries). The latter occur between the multiple coexisting states with (on average) j adsorbed and $(M-j)$ desorbed PE chains. We find the exact parameters of all the subtransitions $((j)\text{-}(M-j)) \to ((j\pm 1)\text{-}(M-j\mp 1))$ and discover splitting of the critical-adsorption boundaries for each of them. These findings extend the previous theoretical and simulations-based results on critical adsorption of a single PE onto the SNP.

Clearly, some important features were neglected in our model (in particular, regarding the physical nature of PE–SNP interactions). Namely, (i) a possibility of a low-dielectric SNP interior, important for PE adsorption onto certain colloids and globular proteins. This feature requires certain modifications of the PE–SNP ES potential [21] and gives rise to a short-range ES repulsion of PEs from the interface. As a result, the critical-adsorption boundary shifts towards *larger* $|\sigma_c|$, as quantified in [21]. The phase-transition splitting discovered above is, however, not expected to be qualitatively affected if the low-dielectric interior is taken into account. (ii) The employed ES-interaction potentials were assumed to be linear in the entire range of solution salinities and SNP charge densities. Naturally, at large $|\sigma|$—when the SNP ES potential becomes $|\psi| \gg 25$ mV—the linear ES theory and the Debye–Hückel potentials will become inapplicable. The analysis of PE–SNP critical adsorption for the nonlinear ES potentials was the topic of our recent study [36].[11] (iii) Although only the cases of $M=2$ and $M=6$ chains were considered in the spherical geometry, the generalization to an arbitrary number of adsorbing PEs of varying length and flexibility as well as simulations in other geometries (cylindrical, Janus particles, etc.) are straightforward. The finiteness of the adsorbing 'particle' and its surface-charge renormalization upon PE adsorption are essential to observe the splitting effects of the critical-adsorption boundary.

What are possible applications of these detailed subtransitions for the scenario of multiple PE chains being ES-attracted to an SNP? One biological motivation to pursue this research is to gain a better understanding of the nanoscale properties of PE complexation and aggregate formation between various PEs and oppositely charged proteins [10–12,24,26,27,67]. Suppression of protein aggregation, protein-purification set-ups and stabilization of proteins against thermal denaturation are possible due to certain coatings involving adsorbed PEs. Other key applications involve protein–PE complexes used as the basic tool for protein-delivery purposes and also for preserving the enzymatic activity [12]. Moreover, for semiflexible SNP-adsorbing PE chains this new approach enables us to revisit the properties of DNA complexation with the histone proteins in the nucleosome core particles [16,49,89], the fundamental units of compactification of genomic DNA in eukaryotic chromatin [90,91]. The effects of varying PE flexibility and pH-sensitive charge states of the system's components are the potential targets for future research.

Data accessibility. This article has no additional data. The electronic supplementary material contains auxiliary figures and video files.

Authors' contributions. D.L.Z.C. and S.J.d.C. carried out computer simulations and performed the statistical data analysis; D.L.Z.C., S.J.d.C., R.M. and A.G.C. conceived and designed the study and drafted and critically revised the manuscript. All authors gave final approval for publication and agree to be held accountable for the work performed herein.

Competing interests. The authors have no competing interests to declare.

Funding. The study was partly funded by the Coordenação de Aperfeiçoamento de Pessoal de Nível Superior, Brazil (CAPES), Finance Code 001. S.J.d.C. thanks the Sao Paulo Research Foundation for financial support (FAPESP, grant no. 2018/01841-2). R.M. acknowledges financial support from the Deutsche Forschungsgemeinschaft (DFG grant no. ME 1535/7-1). R.M. also thanks the Foundation for Polish Science (Fundacja na rzecz Nauki Polskiej) for support within an Alexander von Humboldt Polish Honorary Research Scholarship.

Acknowledgements. The simulations were performed using the resources of the Center for Scientific Computing (NCC/GridUNESP), the Sao Paulo State University, Brazil.

Endnotes

[1]The dielectric permittivity inside globular proteins is typically rather low, $\epsilon_s \sim 2 \ldots 10$; it can be a complicated function of protein dimensions, hydrophobicity of the protein core, protein shape, density and positioning of charges on its surface [92,93], etc. Critical PE adsorption onto low-dielectric interfaces is known to demand higher surface-charge densities, particularly in the low-salt limit (see [21]).

[2]Note that, owing to the presence of own PEs and SNP counterions, the effective solution salinity never drops to zero, even if no added salt is present, $n_0 = 0$. The effect of own counterions on the effective κ value is, however, fairly small because of a large simulation cell/box chosen in the model. For instance, for a relatively large net electric charge present in the PEs–SNP system at no added salt (with $M = 2$ chains, at $\sigma = -0.1$ C m^{-2} for the SNP and at $n_0 = 0$), the counterion-mediated screening yields $\kappa a \approx 0.04$. This value is about 10 times smaller than the smallest κa values shown on the horizontal axis of figure 5.

[3]For crankshaft motions, two arbitrary PE monomers are chosen at random in the simulations defining an axis for rotation. All the monomers along the PE contour between the chosen two are then rotated around this imaginary axis by a random angle [88,94]. As we do not execute displacements of single polymer monomers, the crankshaft motions and pivot movements used in our scheme are vital to modify and efficiently sample all possible polymer conformations, both close to the adsorbing SNP and for relatively free chains in the solution. Pivot rotations and displacements of the entire polymer chain can be performed more frequently without greatly increasing the total simulation time. With this strategy, the best sampling in the region of coexistence conditions could be achieved (for a fixed inter-monomer distance along the PE contour, l_B, meaning non-stretchable chains). Note that, close to the transition point, both the states of the PEs in the adsorbed (close to the nanosphere) and desorbed states (far from the SNP) need to be sampled properly. The motions of the whole polymer in our simulation scheme, therefore, become particularly important near the adsorption–desorption boundary at which certain 'jumps' across the energy barriers separating the two states take place particularly often.

[4]Namely, at $|\sigma| < |\sigma_c|$ the PE chains are in the desorbed state and their ES attraction energy to the SNP is insufficient to overcome the entropic preference to stay free/unbound in the solution. By contrast,

at $|\sigma| > |\sigma_c|$ the ES energy of PE–SNP attraction overwhelms the entropic contribution and the chains stay in adsorbed configurations in the SNP vicinity (the adsorbed state).

[5]We avoid any ambiguous Gaussian-based fitting of the respective probability distributions of the partially adsorbed states. We also assume that transitions occur only between the *neighbouring* substates: the relatively large adsorption energy for each additional PE being adsorbed justifies this assumption. Namely, the energy states are then often well separated, so the exchange between the *neighbouring* states is expected to dominate the state-exchange dynamics.

[6]The data in electronic supplementary material, figure S4 are obtained via calculating the ES binding-energy fluctuations for a subset of polymer configurations in which the PE chains are in one of the two adsorption substates (referring to the respective adsorption–desorption transition). For example, for the subtransition (2-0)→(1-1) we select just those polymer configurations yielding either two or one PE chains being adsorbed onto the nanosphere. Note that for large amounts of added salt the mean ES PE–SNP binding energy is relatively weak: for instance, for $n_0 = 0.5$ M we get $\langle E_B \rangle = -0.13 \pm 1.76\, k_BT$, but still there exist few polymer configurations for which the ES-energy fluctuations are detected to be rather large (see also electronic supplementary material, figure S5 for the energy-fluctuation-based results for the case of six adsorbing chains).

[7]The error bars in figure 4*b*, in the lower subpanels of each panel in electronic supplementary material, figure S5 and in electronic supplementary material, figure S6*b* were calculated via dividing the entire data series for the polymer trajectories obtained from simulations into three equal parts, calculating the degree of energy fluctuations for each of the parts and finally evaluating the standard deviation of these three values to obtain the magnitude of the respective error bars (for a given set of model parameters).

[8]The double-crossing found for, for example the (5-1) and (4-2) probability distribution curves in electronic supplementary material, figure S6*a*, is a reflection of the increasing trend in $|\sigma_c|$ at small salinities: we thus have two critical κ values for the same $|\sigma|$ value. The probability distributions for some neighbouring PE substates are bimodal and cross each other at *two distinct* values of κ. Specifically, for the (4-2) substate in the high-κ regime the PEs mainly 'feel' the mean ES potential of the sphere. As κ decreases, the (5-1) substate becomes more stable (having larger probabilities of occurrence) owing to reduced ES screening. When κ drops below $\approx$0.02 the ES repulsion of the adsorbed PEs becomes important and the (5-1) substate becomes unstable, while at the same time the probability of the (4-2) substate increases again.

[9]We note also that in the high-charge and low-salt limit—owing to strong ES PE–PE repulsion (along the sphere surface and across its interior)—the PE configurations in the adsorbed states observed in the simulations are not azimuthally random. The PE chains are rather adsorbed in somewhat ordered patterns in order to stay away from the neighbouring adsorbed PEs (see also [40,59,89,95,96]). Adsorbed PE chains can thereby form peculiar geometric structures similar to a Wigner crystal [97] (see figure 1 and the video files at low salt in the electronic supplementary material). This is a reflection of the Thompson problem of minimization of the screened Coulomb ES energy, manifesting itself, for example, as boundary scars in the spherical crystallography [98].

[10]For the conditions of the current study, this increasing trend at low κ does not occur for the (1-5)–(0-6) subtransition: because of this no splitting of the adsorption–desorption boundary was detected in our previous studies of single-PE adsorption onto the oppositely charged sphere. Potentially, however, the increasing trend of $|\sigma_c(n_0)|$ at small salinities is realizable also for single-chain PE–SNP adsorption. Various model parameters such as the linear PE charge density, PE length, sphere radius and charge ratio η should be varied to detect such a splitting behaviour. One can imagine, for example, a long weakly charged PE chain that winds around the attractive SNP: in this adsorbed state, at low-salt conditions the PE gradually increasing in length will experience similar effects of intersegmental PE–PE ES repulsions as intra-PE repulsions for adsorption of multiple PE chains onto the SNP. The computer-simulation-based analysis of this problem is currently underway.

[11]The differences in the critical-adsorption conditions obtained for the exponentially screened PE–SNP ES potential were observed in the nonlinear model [36] only at high surface-charge densities and for elevated salt concentrations. By contrast, the effects of splitting of $|\sigma_c|$ versus κ adsorption boundary is observed at low SNP surface-charge densities and in the regime of low salt (figure 5). The effect of splitting of the adsorption–desorption boundary is, therefore, expected to be present also for nonlinear Poisson–Boltzmann PE–SNP potentials. Note that for the highly charged SNP the concept of charge renormalization can be implemented to reduce the 'effective' SNP surface-charge density that interacts with the PEs. Thereby, this will extend the region of model parameters where the linear Poisson–Boltzmann theory is still applicable for computing the critical-adsorption conditions of multiple adsorbing PEs.

References

1. Netz RR, Andelman D. 2003 Neutral and charged polymers at interfaces. *Phys. Rep.* **380**, 1–95. (doi:10.1016/S0370-1573(03)00118-2)
2. Muthukumar M. 1987 Adsorption of a polyelectrolyte chain to a charged surface. *J. Chem. Phys.* **86**, 7230–7235. (doi:10.1063/1.452763)
3. Dobrynin AV, Rubinstein M. 2005 Theory of polyelectrolytes in solutions and at surfaces. *Progr. Pol. Sci.* **30**, 1049–1118. (doi:10.1016/j.progpolymsci.2005.07.006)
4. Dobrynin AV. 2008 Theory and simulations of charged polymers: from solution properties to polymeric nanomaterials. *Curr. Opin. Colloid Interface Sci.* **13**, 376–388. (doi:10.1016/j.cocis.2008.03.006)
5. Szilagyi I, Trefalt G, Tiraferri A, Maroni P, Borkovec M. 2014 Polyelectrolyte adsorption, interparticle forces, and colloidal aggregation. *Soft Matter* **10**, 2479–2502. (doi:10.1039/c3sm52132j)
6. Winkler RG, Cherstvy AG. 2014 Strong and weak polyelectrolyte adsorption onto oppositely charged curved surfaces. In *Polyelectrolyte complexes in the dispersed and solid state I*, vol. 255, pp. 1–56. Berlin, Germany: Springer.
7. McQuigg DW, Kaplan JI, Dubin PL. 1992 Critical conditions for the binding of polyelectrolytes to small oppositely charged micelles. *J. Phys. Chem.* **96**, 1973–1978. (doi:10.1021/j100183a080)
8. Miura N, Dubin PL, Moorefield CN, Newkome GR. 1999 Complex formation by electrostatic interaction between carboxyl-terminated dendrimers and oppositely charged polyelectrolytes. *Langmuir* **15**, 4245–4250. (doi:10.1021/la990125l)
9. Feng XH, Dubin PL, Zhang HW, Kirton GF, Bahadur P, Parotte J. 2001 Critical conditions for binding of dimethyldodecylamine oxide micelles to polyanions of variable charge density. *Macromolecules* **34**, 6373–6379. (doi:10.1021/ma010304l)
10. Cooper CL, Dubin PL, Kayitmazer AB, Turksen S. 2005 Polyelectrolyte–protein complexes. *Curr. Opin. Colloid Interface Sci.* **10**, 52–78. (doi:10.1016/j.cocis.2005.05.007)
11. Cooper CL *et al.* 2006 Effects of polyelectrolyte chain stiffness, charge mobility, and charge sequences on binding to proteins and micelles. *Biomacromolecules* **7**, 1025–1035. (doi:10.1021/bm050592j)
12. Kizilay E, Kayitmazer AB, Dubin PL. 2013 Protein–polyelectrolyte interactions. *Soft Matter* **9**, 2553–2583. (doi:10.1039/c3sm50591j)
13. Wiegel FW. 1977 Adsorption of a macromolecule to a charged surface. *J. Phys. A.* **10**, 299–303. (doi:10.1088/0305-4470/10/2/018)
14. Wiegel FW. 1986 *Introduction to path-integral methods physics and polymer science*. Singapore: World Scientific.
15. von Goeler F, Muthukumar M. 1994 Adsorption of polyelectrolytes onto curved surfaces. *J. Chem. Phys.* **100**, 7796–7803. (doi:10.1063/1.466822)
16. Cherstvy AG, Winkler RG. 2005 Simple model for overcharging of a sphere by a wrapped oppositely charged asymmetrically neutralized polyelectrolyte: possible effects of helical charge distribution. *J. Phys. Chem. B* **109**, 2962–2969. (doi:10.1021/jp0462299)

17. Winkler RG, Cherstvy AG. 2006 Critical adsorption of polyelectrolytes onto charged spherical colloids. *Phys. Rev. Lett.* **96**, 066103. (doi:10.1103/PhysRevLett.96.066103)
18. Winkler RG, Cherstvy AG. 2007 Adsorption of weakly charged polyelectrolytes onto oppositely charged spherical colloids. *J. Phys. Chem. B* **111**, 8486–8493. (doi:10.1021/jp068489r)
19. Hoda N, Kumar S. 2008 Theory of polyelectrolyte adsorption onto surfaces patterned with charge and topography. *J. Chem. Phys.* **128**, 124907. (doi:10.1063/1.2835607)
20. Cherstvy AG, Winkler RG. 2011 Polyelectrolyte adsorption onto oppositely charged interfaces: unified approach for plane, cylinder, and sphere. *Phys. Chem. Chem. Phys.* **13**, 11 686–11 693. (doi:10.1039/c1cp20749k)
21. Cherstvy AG, Winkler RG. 2012 Polyelectrolyte adsorption onto oppositely charged interfaces: image-charge repulsion and surface curvature. *J. Phys. Chem. B* **116**, 9838–9845. (doi:10.1021/jp304980e)
22. Wang J, Muthukumar M. 2011 Encapsulation of a polyelectrolyte chain by an oppositely charged spherical surface. *J. Chem. Phys.* **135**, 194901. (doi:10.1063/1.3662069)
23. Cherstvy AG. 2012 Critical polyelectrolyte adsorption under confinement: planar slit, cylindrical pore, and spherical cavity. *Biopolymers* **97**, 311–317. (doi:10.1002/bip.22023)
24. de Carvalho SJ, Metzler R, Cherstvy AG. 2014 Critical adsorption of polyelectrolytes onto charged Janus nanospheres. *Phys. Chem. Chem. Phys.* **16**, 15539–15550. (doi:10.1039/C4CP02207F)
25. de Carvalho SJ, Metzler R, Cherstvy AG. 2015 Inverted critical adsorption of polyelectrolytes in confinement. *Soft Matter* **11**, 4430–4443. (doi:10.1039/C5SM00635J)
26. Mattison KW, Dubin PL, Brittain IJ. 1998 Complex formation between bovine serum albumin and strong polyelectrolytes: effect of polymer charge density. *J. Phys. Chem. B* **102**, 3830–3836. (doi:10.1021/jp980486u)
27. Seyrek E, Dubin PL, Tribet C, Gamble EA. 2003 Ionic strength dependence of protein-polyelectrolyte interactions. *Biomacromolecules* **4**, 273–282. (doi:10.1021/bm025664a)
28. Mishael YG, Dubin PL, de Vries R, Kayitmazer AB. 2007 Effect of pore size on adsorption of a polyelectrolyte to porous glass. *Langmuir* **23**, 2510–2516. (doi:10.1021/la062314r)
29. Kizilay E, Kayitmazer AB, Dubin PL. 2011 Complexation and coacervation of polyelectrolytes with oppositely charged colloids. *Adv. Coll. Interface Sci.* **167**, 24–37. (doi:10.1016/j.cis.2011.06.006)
30. Sennato S, Truzzolillo D, Bordi F. 2012 Aggregation and stability of polyelectrolyte-decorated liposome complexes in water-salt media. *Soft Matter* **8**, 9384–9395. (doi:10.1039/c2sm25576f)
31. Sennato S, Carlini L, Truzzolillo D, Bordi F. 2016 Salt-induced reentrant stability of polyion-decorated particles with tunable surface charge density. *Coll. Surf. B: Biointerf.* **137**, 109–120. (doi:10.1016/j.colsurfb.2015.06.011)
32. Kong CY, Muthukumar M. 1998 Monte Carlo study of adsorption of a polyelectrolyte onto charged surfaces. *J. Chem. Phys.* **109**, 1522–1527. (doi:10.1063/1.476703)
33. de Carvalho SJ. 2010 First-order–like transition in salt-induced macroion–polyelectrolyte desorption. *Europhys. Lett.* **92**, 18001. (doi:10.1209/0295-5075/92/18001)
34. de Carvalho SJ, Caetano DLZ. 2013 Adsorption of polyelectrolytes onto oppositely charged cylindrical macroions. *J. Chem. Phys.* **138**, 244909. (doi:10.1063/1.4811842)
35. de Oliveira VM, de Carvalho SJ. 2014 Adsorption of pH-responsive polyelectrolyte chains onto spherical macroions. *Eur. Phys. J. E* **37**, 75. (doi:10.1140/epje/i2014-14075-4)
36. de Carvalho SJ, Metzler R, Cherstvy AG. 2016 Critical adsorption of polyelectrolytes onto planar and convex highly charged surfaces: the nonlinear Poisson–Boltzmann approach. *New. J. Phys.* **18**, 083037. (doi:10.1088/1367-2630/18/8/083037)
37. Landsgesell J, Nová L, Rud O, Uhlík F, Sean D, Hebbeker P, Holm C, Košovan P. 2019 Simulations of ionization equilibria in weak polyelectrolyte solutions and gels. *Soft Matter* **15**, 1155–1185. (doi:10.1039/C8SM02085J)
38. Netz RR, Joanny JF. 1998 Complexation behavior of polyampholytes and charged objects. *Macromolecules* **31**, 5123–5141. (doi:10.1021/ma980115b)
39. Netz RR, Joanny JF. 1999 Adsorption of semiflexible polyelectrolytes on charged planar surfaces: charge compensation, charge reversal, and multilayer formation. *Macromolecules* **32**, 9013–9025. (doi:10.1021/ma990263h)
40. Kunze KK, Netz RR. 2000 Salt-induced DNA-histone complexation. *Phys. Rev. Lett.* **85**, 4389. (doi:10.1103/PhysRevLett.85.4389)
41. Dobrynin AV, Deshkovski A, Rubinstein M. 2001 Adsorption of polyelectrolytes at oppositely charged surfaces. *Macromolecules* **34**, 3421–3436. (doi:10.1021/ma0013713)
42. Jonsson M, Linse P. 2001 Polyelectrolyte–macroion complexation. I. Effect of linear charge density, chain length, and macroion charge. *J. Chem. Phys.* **115**, 3406–3418. (doi:10.1063/1.1385792)
43. Stoll S, Chodanowski P. 2001 Polyelectrolyte adsorption on charged particles: ionic concentration and particle size effects—a Monte Carlo approach. *J. Chem. Phys.* **115**, 4951–4960. (doi:10.1063/1.1392357)
44. Chodanowski P, Stoll S. 2001 Polyelectrolyte adsorption on charged particles in the Debye-Hückel approximation. A Monte Carlo approach. *Macromolecules* **34**, 2320–2328. (doi:10.1021/ma000482z)
45. Ellis M, Kong CY, Muthukumar M. 2000 Polyelectrolyte adsorption on heterogeneously charged surfaces. *J. Chem. Phys.* **112**, 8723–8729. (doi:10.1063/1.481474)
46. Stoll S, Chodanowski P. 2002 Polyelectrolyte adsorption on an oppositely charged spherical particle. Chain rigidity effects. *Macromolecules* **35**, 9556–9562. (doi:10.1021/ma020272h)
47. Akinchina A, Linse P. 2002 Monte Carlo simulations of polyion-macroion complexes. 1. Equal absolute polyion and macroion charges. *Macromolecules* **35**, 5183–5193. (doi:10.1021/ma012052u)
48. Messina R. 2003 Adsorption of oppositely charged polyelectrolytes onto a charged rod. *J. Chem. Phys.* **119**, 8133–8139. (doi:10.1063/1.1609193)
49. Schiessel H. 2003 The physics of chromatin. *J. Phys.: Cond. Matt.* **15**, R699. (doi:10.1088/0953-8984/15/19/203)
50. Cherstvy AG, Winkler RG. 2004 Complexation of semiflexible chains with oppositely charged cylinder. *J. Chem. Phys.* **120**, 9394–9400. (doi:10.1063/1.1707015)
51. Ulrich S, Laguecir A, Stoll S. 2004 Complex formation between a nanoparticle and a weak polyelectrolyte chain: Monte Carlo simulations. *J. Nanopart. Res.* **6**, 595–603. (doi:10.1007/s11051-004-3548-4)
52. De Vries R. 2004 Monte Carlo simulations of flexible polyanions complexing with whey proteins at their isoelectric point. *J. Chem. Phys.* **120**, 3475–3481. (doi:10.1063/1.1641003)
53. Messina R, Holm C, Kremer K. 2003 Polyelectrolyte multilayering on a charged sphere. *Langmuir* **19**, 4473–4482. (doi:10.1021/la026988n)
54. Carrillo JMY, Dobrynin AV. 2007 Molecular dynamics simulations of polyelectrolyte adsorption. *Langmuir* **23**, 2472–2482. (doi:10.1021/la063079f)
55. Messina R, Holm C, Kremer K. 2004 Polyelectrolyte adsorption and multilayering on charged colloidal particles. *J. Polymer Sci.: Part B* **42**, 3557–3570. (doi:10.1002/polb.20203)
56. Messina R. 2004 Polyelectrolyte multilayering on a charged planar surface. *Macromolecules* **37**, 621–629. (doi:10.1021/ma034689e)
57. Ulrich S, Laguecir A, Stoll S. 2005 Complexation of a weak polyelectrolyte with a charged nanoparticle. Solution properties and polyelectrolyte stiffness influences. *Macromolecules* **38**, 8939–8949. (doi:10.1021/ma051142m)
58. Shafir A, Andelman D. 2006 Polyelectrolyte multilayer formation: electrostatics and short-range interactions. *Eur. Phys. J. E* **19**, 155–162. (doi:10.1140/epje/e2006-00018-3)
59. Cherstvy AG, Winkler RG. 2006 Strong and weak adsorption of polyelectrolyte chains onto oppositely charged spheres. *J. Chem. Phys.* **125**, 064904. (doi:10.1063/1.2229205)
60. Ulrich S, Seijo M, Stoll S. 2006 The many facets of polyelectrolytes and oppositely charged macroions complex formation. *Curr. Opin. Coll. Interface Sci.* **11**, 268–272. (doi:10.1016/j.cocis.2006.08.002)
61. Messina R. 2009 Electrostatics in soft matter. *J. Phys.: Cond. Matt.* **21**, 113102. (doi:10.1088/0953-8984/21/11/113102)
62. Carnal F, Stoll S. 2011 Adsorption of weak polyelectrolytes on charged nanoparticles. Impact of salt valency, pH, and nanoparticle charge density. Monte Carlo simulations. *J. Phys. Chem. B* **115**, 12007–12018. (doi:10.1021/jp205616e)
63. Ulrich S, Seijo M, Carnal F, Stoll S. 2011 Formation of complexes between nanoparticles and weak

polyampholyte chains. Monte Carlo simulations. *Macromolecules* **44**, 1661–1670. (doi:10.1021/ma1024895)

64. Yigit C, Heyda J, Ballauff M, Dzubiella J. 2015 Like-charged protein-polyelectrolyte complexation driven by charge patches. *J. Chem. Phys.* **143**, 064905. (doi:10.1063/1.4928078)
65. Stornes M, Linse P, Dias R. 2017 Monte Carlo simulations of complexation between weak polyelectrolytes and a charged nanoparticle. Influence of polyelectrolyte chain length and concentration. *Macromolecules* **50**, 5978–5988. (doi:10.1021/acs.macromol.7b00844)
66. Shojaei HR, Muthukumar M. 2017 Adsorption and encapsulation of flexible polyelectrolytes in charged spherical vesicles. *J. Chem. Phys.* **146**, 244901. (doi:10.1063/1.4986961)
67. Nash JA, Kwansa AL, Peerless JS, Kim HS, Yingling YG. 2017 Advances in molecular modeling of nanoparticle–nucleic acid interfaces. *Bioconjugate Chem.* **28**, 3–10. (doi:10.1021/acs.bioconjchem.6b00534)
68. Nunes SCC, Cova TFGG, Dias RS, Pais AACC. 2018 Adsorption of charged macromolecules upon multicomponent responsive surfaces. *Phys. Chem. Chem. Phys.* **20**, 19811–19818. (doi:10.1039/C8CP03383H)
69. Tagliabue A, Izzo L, Mella M. 2019 Absorbed weak polyelectrolytes: impact of confinement, topology, and chemically specific interactions on ionization, conformation free energy, counterion condensation, and absorption equilibrium. *J. Polym. Sci. Part B* **57**, 491–510. (doi:10.1002/polb.24806)
70. Muthukumar M. 1995 Pattern recognition by polyelectrolytes. *J. Chem. Phys.* **103**, 4723–4731. (doi:10.1063/1.470691)
71. McNamara J, Kong CY, Muthukumar M. 2002 Monte Carlo studies of adsorption of a sequenced polyelectrolyte to patterned surfaces. *J. Chem. Phys.* **117**, 5354–5360. (doi:10.1063/1.1501125)
72. Nunes SCC, Pinto P, Pais AACC. 2013 Nonrandom adsorption of polyelectrolyte chains on finite regularly charged surfaces. *J. Comp. Chem.* **34**, 1198–1209. (doi:10.1002/jcc.23238)
73. Samanta R, Halabe A, Ganesan V. 2020 Influence of charge regulation and charge heterogeneity on complexation between polyelectrolytes and proteins. *J. Phys. Chem. B*. **124**, 4421. (doi:10.1021/acs.jpcb.0c02007)
74. Messina R. 2004 Effect of image forces on polyelectrolyte adsorption at a charged surface. *Phys. Rev. E* **70**, 051802. (doi:10.1103/PhysRevE.70.051802)
75. dos Santos AP, Girotto M, Levin Y. 2016 Simulations of polyelectrolyte adsorption to a dielectric like-charged surface. *J. Phys. Chem. B* **120**, 10387–10393. (doi:10.1021/acs.jpcb.6b06002)
76. Mella M, Izzo L. 2017 Modulation of ionization and structural properties of weak polyelectrolytes due to 1D, 2D, and 3D confinement. *J. Polym. Sci. Part B: Polym. Phys.* **55**, 1088–1102. (doi:10.1002/polb.24351)
77. Mella M, Tagliabue A, Mollica L, Izzo L. 2020 Monte Carlo study of the effects of macroion charge distribution on the ionization and adsorption of weak polyelectrolytes and concurrent counterion release. *J. Coll. Interface Sci.* **560**, 667–680. (doi:10.1016/j.jcis.2019.10.051)
78. Caetano DLZ, de Carvalho SJ. 2017 Conformational properties of block-polyampholytes adsorbed on charged cylindrical surfaces. *Eur. Phys. J. E* **40**, 33. (doi:10.1140/epje/i2017-11525-5)
79. Caetano DLZ, de Carvalho SJ, Metzler R, Cherstvy AG. 2017 Critical adsorption of periodic and random polyampholytes onto charged surfaces. *Phys. Chem. Chem. Phys.* **19**, 23 397–23 413. (doi:10.1039/C7CP04040G)
80. Wang Y, Dubin PL, Zhang H. 2001 Interaction of DNA with cationic micelles: effects of micelle surface charge density, micelle shape, and ionic strength on complexation and DNA collapse. *Langmuir* **17**, 1670–1673. (doi:10.1021/la0010673)
81. Frauenrath H. 2005 Dendronized polymers—building a new bridge from molecules to nanoscopic objects. *Prog. Polym. Sci.* **30**, 325–384. (doi:10.1016/j.progpolymsci.2005.01.011)
82. Angelescu DG. 2019 Coarse-grained simulation studies on the adsorption of polyelectrolyte complexes upon lipid membranes. *Phys. Chem. Chem. Phys.* **21**, 12 446–12 459. (doi:10.1039/C9CP01448A)
83. Luque-Caballero G, Maldonado-Valderrama J, Quesada-Perez M, Martin-Molina A. 2019 Interaction of DNA with likely-charged lipid monolayers: an experimental study. *Colloids Surf. B Biointerfaces* **178**, 170–176. (doi:10.1016/j.colsurfb.2019.02.058)
84. Cherstvy AG, Petrov EP. 2014 Modeling DNA condensation on freestanding cationic lipid membranes. *Phys. Chem. Chem. Phys.* **16**, 2020–2037. (doi:10.1039/C3CP53433B)
85. Cherstvy AG. 2007 Electrostatics of DNA complexes with cationic lipid membranes. *J. Phys. Chem. B* **111**, 7914–7927. (doi:10.1021/jp0700175)
86. Koltover I, Wagner K, Safinya CR. 2000 DNA condensation in two dimensions. *Proc. Natl Acad. Sci. USA* **97**, 14 046–14 051. (doi:10.1073/pnas.97.26.14046)
87. de Carvalho SJ, Ghiotto RCT. 2006 Monte Carlo and modified Tanford–Kirkwood results for macromolecular electrostatics calculations. *J. Phys. Chem. B* **110**, 8832–8839. (doi:10.1021/jp054891e)
88. Attig N, Binder K, Grubmüller H, Kremer K. 2004 *Computational soft matter: from synthetic polymers to proteins*. Jülich, Germany: John von Neumann Institute for Computing (NIC).
89. Cherstvy A. 2011 Electrostatic interactions in biological DNA-related systems. *Phys. Chem. Chem. Phys.* **13**, 9942–9968. (doi:10.1039/c0cp02796k)
90. Schalch T, Duda S, Sargent DF, Richmond TJ. 2005 X-ray structure of a tetranucleosome and its implications for the chromatin fibre. *Nature* **436**, 138–141. (doi:10.1038/nature03686)
91. Luger K, Dechassa ML, Tremethick DJ. 2012 New insights into nucleosome and chromatin structure: an ordered state or a disordered affair? *Nat. Rev. Mol. Cell Biol.* **13**, 436–447. (doi:10.1038/nrm3382)
92. Schutz CN, Warshel A. 2001 What are the dielectric 'constants' of proteins and how to validate electrostatic models? *Proteins* **44**, 400–417. (doi:10.1002/prot.1106)
93. Li L, Li C, Zhang Z, Alexov E. 2013 On the dielectric 'constant' of proteins: smooth dielectric function for macromolecular modeling and its implementation in DelPhi. *J. Chem. Theory Comput.* **9**, 2126–2136. (doi:10.1021/ct400065j)
94. Binder K. 1995 *Monte Carlo and molecular dynamics simulations in polymer science*. Oxford, UK: Oxford University Press.
95. Boroudjerdi H, Naji A, Netz RR. 2014 Global analysis of the ground-state wrapping conformation of a charged polymer on an oppositely charged nano-sphere. *Eur. Phys. J. E* **37**, 21. (doi:10.1140/epje/i2014-14021-6)
96. Chaurasia V, Chen YC, Fried E. 2020 Interacting charged elastic loops on a sphere. *J. Mech. Phys. Solids* **134**, 103771. (doi:10.1016/j.jmps.2019.103771)
97. Grosberg AY, Nguyen TT, Shklovskii BI. 2002 Colloquium: The physics of charge inversion in chemical and biological systems. *Rev. Mod. Phys.* **74**, 329–345. (doi:10.1103/RevModPhys.74.329)
98. Bausch AR, Bowick MJ, Cacciuto A, Dinsmore AD, Hsu MF, Nelson DR, Nikolaides MG, Travesset A, Weitz DA. 2003 Grain boundary scars and spherical crystallography. *Science* **299**, 1716–1718. (doi:10.1126/science.1081160)